An investigation of modelling approaches for material instability of aluminum sheet metal using the GISSMO-model

Georg Falkinger[1], Nikolay Sotirov[1], Peter Simon[2]

[1]LKR Leichtmetallkompetenzzentrum Ranshofen GmbH, Ranshofen, AT
[2]AMAG rolling GmbH, Ranshofen, AT

1 Abstract

The most generally accepted tool for the assessment of formability of sheet material up to the present date is the forming limit diagram (FLD). It allows the identification of critical areas in a sheet-forming simulation where critical thinning or the appearance of cracks is to be expected. The FLD is determined experimentally in Nakajima tests and is widely used in the design of sheet forming processes. However it is known that the assessment based on the FLD is incomplete. Cracks are observed also in areas, which should be safe according to the FLD and vice versa.

There is a strong need for numerical methods, which allow exact quantitative predictions about critical areas in the sheet forming process. Literature investigations have shown that FE-Analysis in combination with advanced material models constitutes a reliable supplement to the FLD. The General Incremental Stress State dependent Material Model (GISSMO) in LS-Dyna offers the description of necking, damage and failure for sheet materials under complex loading conditions.

Within a joint research project between AMAG rolling GmbH and LKR an advanced concept (GISSMO-Modelling) for the assessment of sheet forming processes was compared to the standard method (FLD). The relevant mechanical properties were determined experimentally und a material card for GISSMO was calibrated. The Validation of the material model was carried out and the predictive quality of the two concepts was compared systematically.

The results of the present paper show, that the use of the GISSMO model leads to a good prediction of the maximum drawing depth of the cross-tool test. The location of fracture was also predicted correctly. The assessment based on the FLD is too conservative. The location of fracture was determined, but the maximum drawing depth according to the FLD is 30% below the measured one. Simulations with different mesh sizes were performed and validated.

2 Introduction

The use of components made of aluminum sheet in the automobile industry is a continuous trend, driven by the constant need for weight reduction. In parallel, the role played by numerical methods for the process- and component- design is gaining importance. Suppliers of aluminum sheet are facing the challenge to (i) optimize the material formability, and (ii) demonstrate the feasibility of complex component geometries within a tight time schedule. The *r*- and *n*-values as well as the experimentally determined FLD e.g. according to the DIN EN ISO 12004 standard do not always guarantee a reliable assessment for these tasks. Therefore validated numerical methods are required (Fig. 1). Subject of the present investigations was a 6xxx series aluminum alloy in T4 temper with a sheet thickness of 2mm.
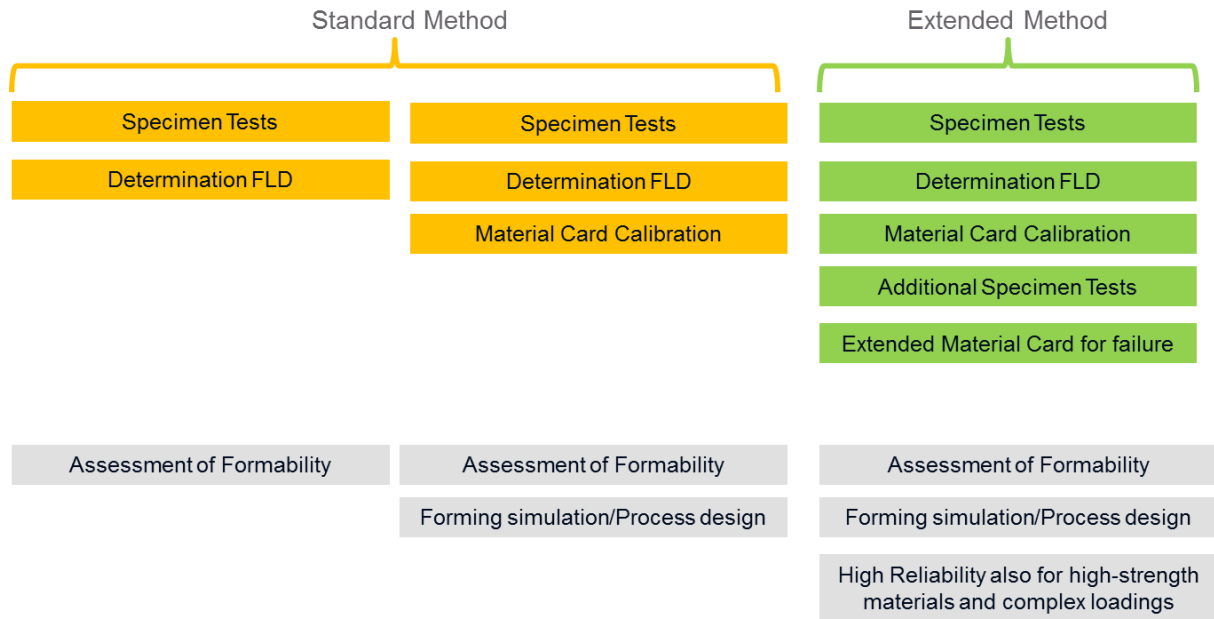
Fig.1: Schematic description of the different methods for the assessment of formability and process design in sheet forming of aluminum alloys investigated in this paper.

3 Ductile damage

Failure of ductile sheet materials under mechanical loading results from a combination of micromechanical mechanisms, which are schematically depicted in Fig. 2. In the first stage, pores develop during deformation. The voids preferably nucleate at large precipitates or other potential nuclei, where stress localizations and strain incompatibilities occur. Void growth, which is driven by further loading, crucially depends on the local stress state. As a rule of thumb, the higher the stress-triaxiality, the faster do the voids grow. A macroscopic crack occurs, when the void volume and distribution reaches a critical state, and the ligaments between the voids are no longer capable to carry the applied load. This formation of micro-cracks and local necks in the ligaments is called void coalescence.
Under shear loadings the fracture mechanisms is slightly modified. In this case, low stress-triaxialities do not lead to an increase in the void volume fraction, The damaged area however increases with deformation. Coalescence between voids occurs in a narrow shear band (cf. Fig. 2).

I. Void growth and coalescence under hydrostatic tension

Hydrostatic stress state | Void nucleation | Void growth | Coalescence
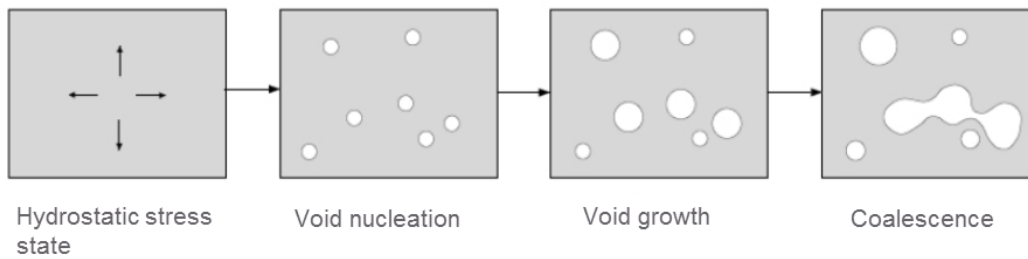
II. Void-Sheeting under Shear

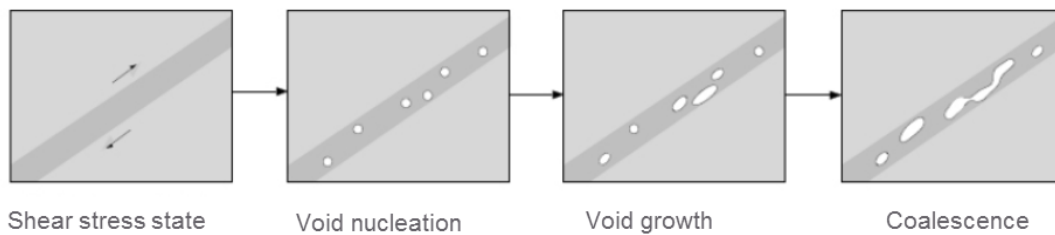Shear stress state | Void nucleation | Void growth | Coalescence

Fig.2: *Schematic description of failure mechanisms at high (upper row) and low (lower row) stress-triaxialities (Source: [1]).*

4 Failure modelling with GISSMO

The damage and failure model GISSMO ([2],[3]) allows a simplified and efficient phenomenological description of ductile damage and failure. The numerical description is based on a scalar damage variable $D \in [0; 1]$, which obeys the following evolution equation:

$$\dot{D} = \frac{n}{\varepsilon_f} D^{\left(1 - \frac{1}{n}\right)} \dot{\varepsilon}_{pl} \tag{1}$$

Here, $\dot{\varepsilon}_{pl}$ is the plastic equivalent strain rate, n the so-called damage exponent and ε_f the fracture strain. When the damage variable reaches a value of 1 at an integration point, the load-carrying capacity is set to zero. The fracture strain ε_f depends on the stress-triaxiality

$$\eta = \frac{p}{\sigma_M} \tag{2}$$

with the hydrostatic pressure $p = -\frac{1}{3}(\sigma_{11} + \sigma_{22} + \sigma_{33})$ and the equivalent Mises-stress σ_M. $\varepsilon_f(\eta)$ constitutes the so called fracture curve, which describes the different void growth rates in dependence of the stress state in a phenomenological way.

5 Experimental characterization and calibration of a material card

Material modelling in sheet stamping requires the correct description of the plastic material behaviour. This includes the determination of the anisotropic yield surface and the yield curve up to high strains. For the present purpose, the yield curve was determined from the uniaxial tensile test in combination with inverse FE modelling. Fig. 3 shows a comparison of the thus found yield curve with the experimentally determined one from a bulge test. For the anisotropic yield surface, a standard-model according to Barlat et al. ([3],[4],[5]) was employed. The corresponding parameters of the chosen model were fitted to r-values in three different directions (0°, 45° and 90° from the rolling direction), cf. Fig. 4.
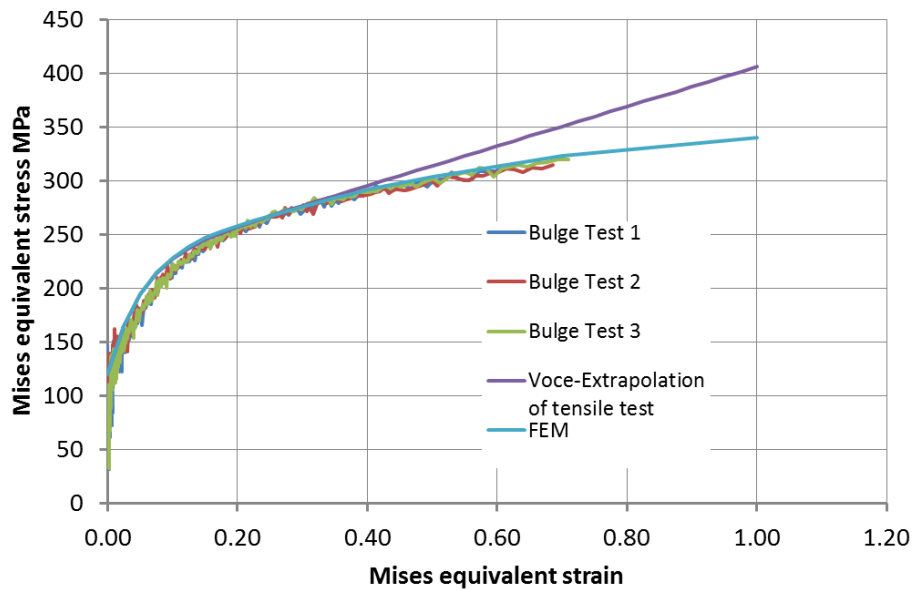
Fig.3: Yield curves at high strains: The analytical Extrapolation according to Voce (violet) over-estimates the hardening behavior. The curve obtained by inverse simulation of the tensile test (light blue) in in good accordance with the experimentally determined one from the bulge test.
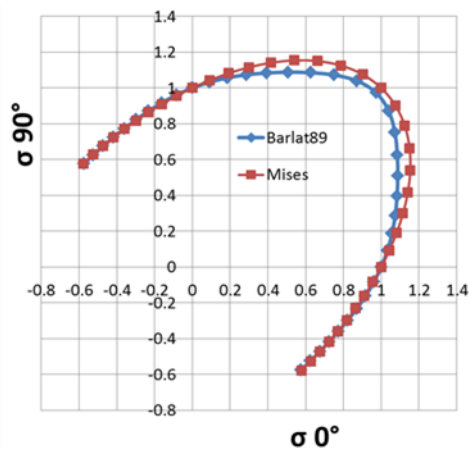

Fig.4: Anisotropic yield surface according to Barlat '89 in comparison to the isotropic Mises-Plasticity.

The calibration of the GISSMO-Model for the description of ductile damage consists essentially in the determination of the fracture curve $\varepsilon_f(\eta)$. For the damage exponent n a standard value of 1.5 was assumed. In order to test different stress-states, tests with different specimen geometries were carried out. By inverse simulation of every single specimen, the fracture curve for the present material could be determined based on 4 interpolated values. An additional interpolation point from the Nakajima test was used for the calibration of the fracture curve in the equi-biaxial regime. Fig. 5 shows the obtained fracture curve.

In the tensile test, the fracture strain was measured experimentally. Furthermore optical measurements of the surface strain field were carried out, using the GOM Aramis system on single specimens. Fig. 6 shows a comparison of different methods to determine the local fracture strain in the flat tensile test and the corresponding result from the inverse FE-Analysis. Neglecting minor deviations all methods are pointing to a value of 0.68 for the local fracture strain.
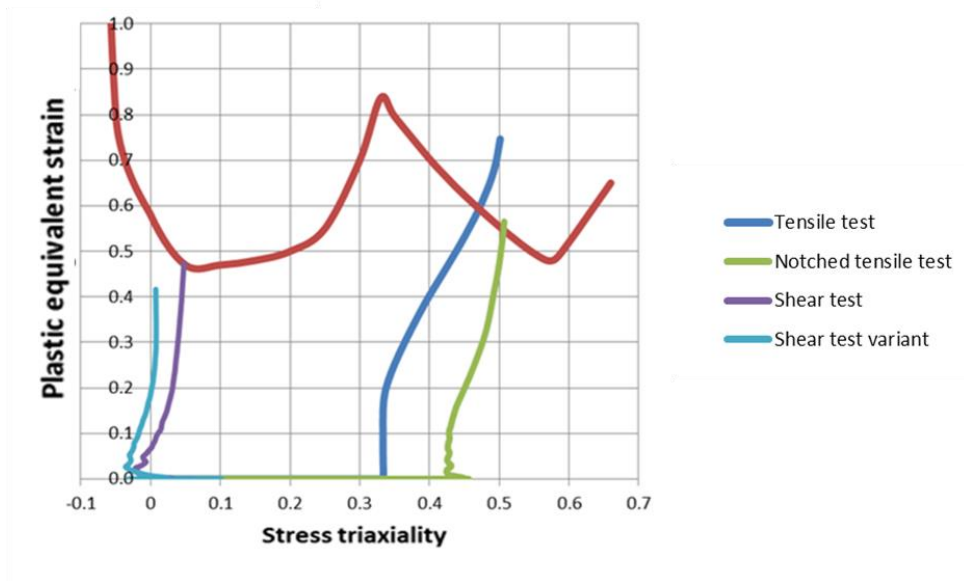
Fig.5:   GISSMO fracture curve (red) and the loading paths from different specimen geometries, as obtained from inverse FEM simulations.
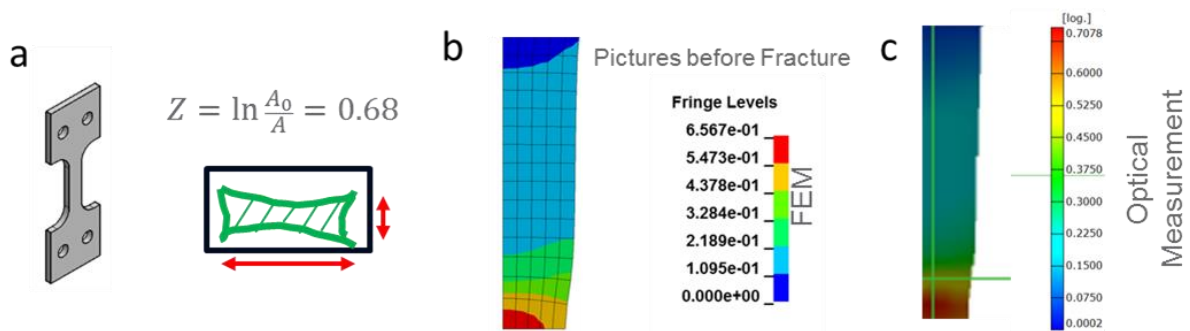

Fig.6:   Comparison of three independent methods to determine the local fracture strain in a flat tensile test. a) Fracture strain measured from the specimen cross-section. Plastic equivalent strains from b) FEM and c) optical measurement of the surface strains with GOM Aramis (note, that in both cases only a quarter of the tensile specimen is represented in the figure.The necked region is at the bottom of the picture).

The validation of the material card for plasticity and failure was based on Nakajima-Tests with five different specimen geometries and the corresponding FLD. Fig. 7 as an example depicts the FE-Model of the Nakajima specimen with a width of 50mm just before fracture. In order to reduce computation time, the symmetry of the model was exploited and only a quarter of the test was modelled. The maximum thickness reduction obviously occurs at the center of the specimen.
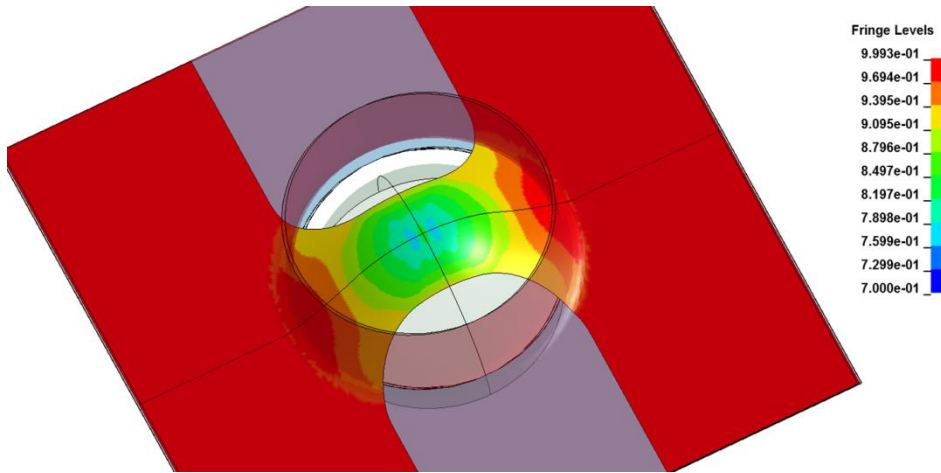
Fig.7: Local distribution of the normalized sheet thickness (1 ≙ 2mm) on a Nakajima specimen with a width of 50mm just before fracture.

Fig. 8 shows a comparison of force-displacement curves from experiment and simulation for specimens with different widths. The evaluation of the Nakajima tests in both experiment and simulation was carried out with two methods: On the one hand the maximum local principal strains were determined. On the other hand the so-called time-method was applied to derive an FLD (cf. Fig. 9). The latter method is represented in [6] and was already successfully used at LKR for an aluminum alloy [7].
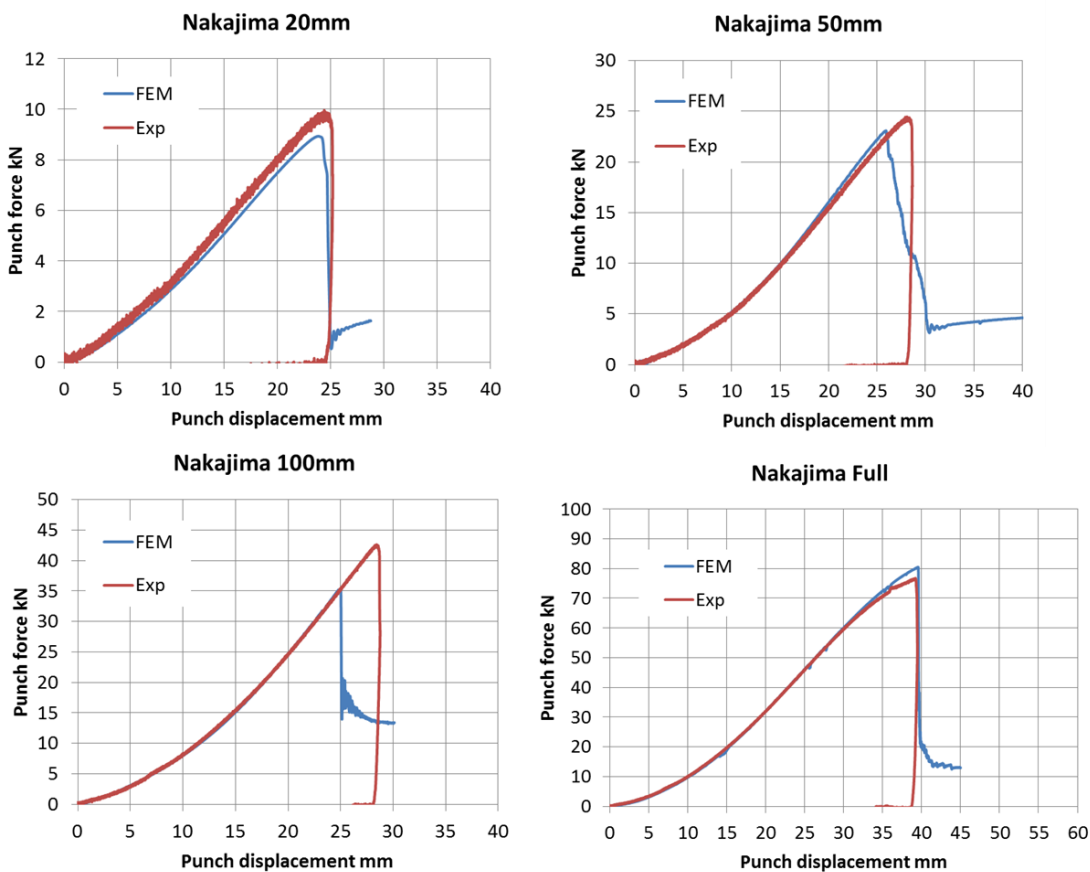

Fig.8: Comparison of experimentally determined force-displacement curves from Nakajima-Tests with different Specimen widths and results from FE-Modelling including failure.
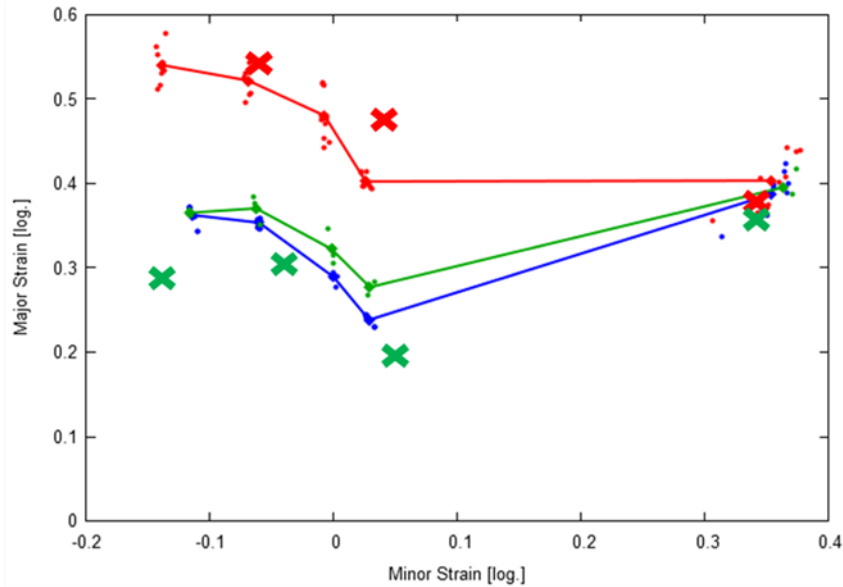
Fig.9: FLD from experiment (small dots) and FEM (crosses). Experimental data was evaluated according to three methods: Maximum local strains (red), DIN EN ISO 12004 section method (blue), time method [6] (green). The maximum local strains and the time method were evaluated from the simulation data in exactly the same way as in the experimental procedure.

Simulations of the specimen tests and the Nakajima tests were carries out with shell elements and an element edge length of 0.5 mm. This fine mesh is necessary to obtain the strain localizations and the local fracture strain after necking. In the industrial application, e.g. the process design of real components, long computation times inhibit the use of a fine mesh of this size. In sheet forming simulations, edge-lengths of 1-2mm are commonly used. The fracture strains, however, which were derived from the specimen tests by inverse FEM are only valid for the mesh size that was used during the calibration. In order to describe the material behavior also for larger mesh sizes, a so called regularization of the fracture curve has to be applied [2]. In the present work, flat tensile tests were used for this purpose. The failure curve is scaled in such a way, that as shown in Fig. 10, the displacement at fracture is correctly predicted with all mesh sizes. In parallel, a coupling of the damage parameter with the flow curve was activated. This procedure is in accordance with the state of art [2].
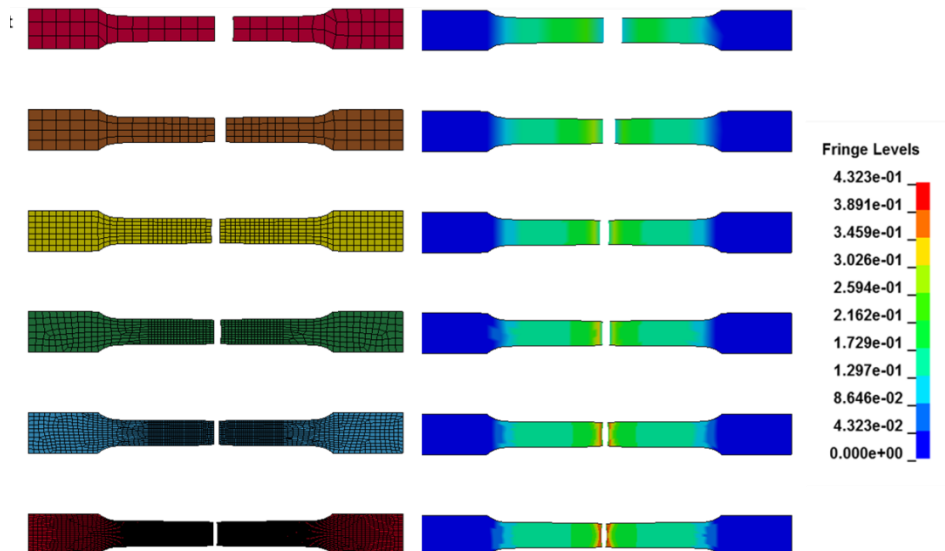

Fig.10: FE-Models of a flat tensile test with different mesh sizes from 0.5mm to 5mm at the same overall displacement. The left column shows the mesh and the right column the distribution of plastic equivalent strain at fracture. Please note the decrease of local strains towards coarser meshes in the necked area. The scaling of the fracture curve in GISSMO compensates this effect.
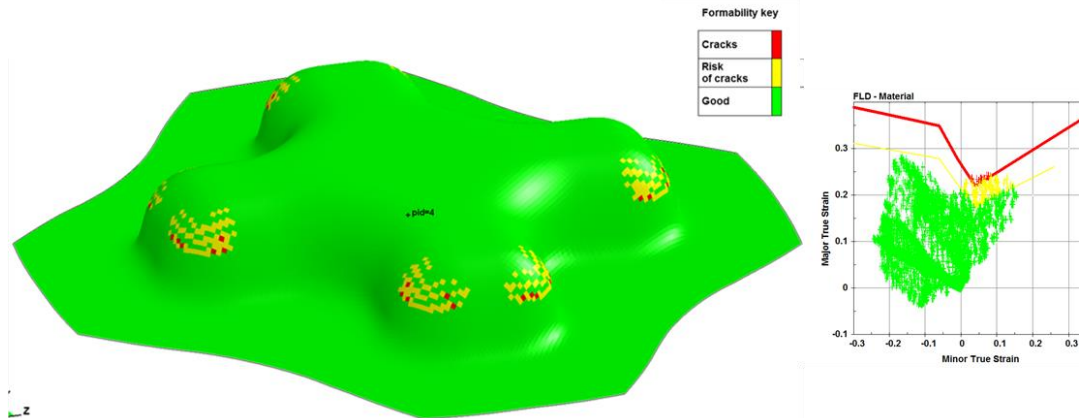
Fig.11: FE Model of the cross-die test at a drawing depth of 32mm. The red points mark the critical areas, where cracks are to be expected. For the assessment, major and minor principal in-plane strains are plotted on the upper sheet surface. The small insert shows a diagram, where the overall strain distribution is compared to the critical forming limit curve derived with the section method. The yellow curve considers a safety margin of 10%.
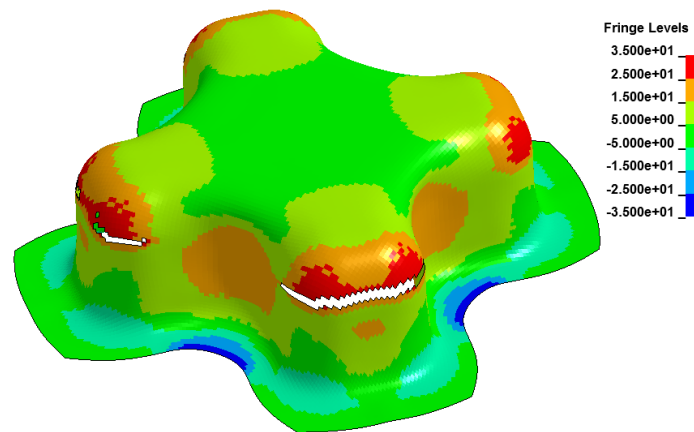

Fig.12: FE-Modell of the cross-die test at a drawing depth of 55mm, just after the appearance of the first crack. The scale shows the sheet thickness reduction in percent.

Fig.13: Cross-die specimen just after rupture. The maximum drawing depth of 53.6 mm was determined in successive trials with constant blank holder force.

6 Cross-die test

For this validation test, plates were drawn in a cross die up to fracture. The maximum drawing depth at the first occurrence of necking and macroscopic cracks was determined in successive trials with a constant blank-holder force. In the FE-Model a friction coefficient of 0.14 was assumed. Fig. 11 and Fig.12 show results from the two assessment methods, FLD and GISSMO respectively. For the evaluation according to the FLD, the major and minor in–plane strains are plotted on the deformed mesh. Points, which lie above the forming limit curve, are expected to be critical areas, where appearance of cracks is highly probable. The results demonstrate that the thus predicted maximum drawing depth of 32mm is too conservative in comparison with the experimental value of 53.6mm (Fig. 13). The drawing depth predicted by the GISSMO model is 55mm and therefore much more precise. Furthermore, the assessment using the FLD is ambiguous, since the user deliberately chooses if the strains are plotted on the upper or the lower surface of the sheet.

7 Instability curves

In order to compensate the mesh-size dependency, the fracture curve was regularized and instability curves [2] for the coupling of damage and yield stress according to Swift [8] and Hill [9] were compared (cf. Fig. 14). The results for different mesh sizes are summarized in Table 1. The results demonstrate that in this case, the Swift-curve yielded good results for all mesh sizes, while the Hill curve slightly underestimates the initiation of failure, except for the finest mesh.

Mesh Size	Hill Maximum Drawing depth	Swift Maximum Drawing depth
0.5mm	53.4 mm	51.5 mm
1mm	56.0 mm	53.8 mm
2mm	59.0 mm	55.8 mm
3mm	56.0 mm	52.7 mm

Table 1: Mesh size dependency of the modelling results. The two different methods for computing the instability curve lead to slightly different results.
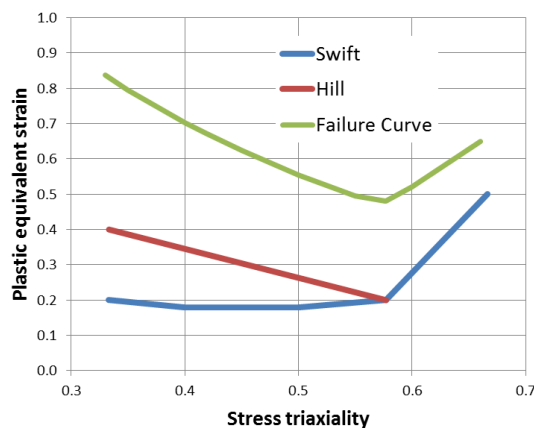

Fig.14: Instability curves according to Swift and Hill. When the plastic strain reaches the instability curve, coupling between the damage parameter and the yield stress is initiated [2],[3].

8 Summary

The essential results from the present work can be summarized as follows:
1. The assessment of the formability according to the forming limit diagram is not always suitable for complex component geometries. In the present case, the prediction was to conservative.
2. The results from FEM using the GISSMO Model in LS-Dyna are in good accordance with the experimental results. The concept of the instability curve

was applied and the mesh-size dependency could be compensated. The instabilitiy curve according to Swift leads to reliable results for common mesh-sizes from 1-3 mm.

9 Acknowledgements

10 Literature

[1] Engelen R.A.B., "Plasitcity induced Damage in Metals", habilitailon thesis, TU Eindhoven, Netherlands, 2005.

[2] Haufe A., DuBois P., Neukamm F., Feucht M., "GISSMO-Material modeling with a sophisticated failure criteria", LS-Dyna Developer Forum, Stuttgart, Germany, 2011.

[3] LS-Dyna Keyword Manual, February 2013, Version 7.0

[4] Barlat F., Lian J., "Plastic behavior and stretchability of sheet metals. Part I: A yield function for orthotropic sheets under plane stress conditions", International Journal of Plasticity, Vol 5 (1), 1989, pp51-66.

[5] Andrieux F., Klitschke S., Böhme W. Sun D.-Z., "Characterization and modeling of the deformation and damage of an aluminum sheet for crash", ICILLS 2014, Cape Town, South Africa.

[6] Merklein M., Kuppert A., Geiger M., "Time dependent determination of forming limit diagrams", CIRP Annals- Manufacturing Technology, Vol 59 (1), 2010, pp 295-298.

[7] Falkinger G., Grabner F., Schneider R., Scheerer M. Sotirov N., "Materials characterization and modelling methods for the cryogenic forming of aluminium alloys", LS-Dyna User Forum, Bamberg, Germany, 2014.

[8] Swift H.W., "Plastic instability under plane stress", Journal of the Mechanics and Physics of Solids, Vol. 1 (1), 1952.

[9] Hill R., "Constitutive modelling of orthotropic plasticity in sheet metal", Journal of the Mechanics and Physics of Solids, Vol. 38 (3), 1990.